Inorg. Chem. **2005**, *44*, 7846–7859

Intramolecular Energy Transfer Involving Heisenberg Spin-Coupled Dinuclear Iron–Oxo Complexes

Laura B. Picraux, Amanda L. Smeigh, Dong Guo, and James K. McCusker*

Department of Chemistry, Michigan State University, East Lansing, Michigan 48824

Received May 2, 2005

The synthesis, structure, and physical properties of a series of oxo-bridged dinuclear Fe(III) complexes containing pendant naphthalene groups are described. The compounds $[Fe_2O(O_2CCH_2–C_{10}H_7)(tren)_2](BPh_4)(NO_3)_2$ (**8**), $[Fe_2O(O_2CCH_2–C_{10}H_7)(TPA)_2](ClO_4)_3$ (**9**), $Fe_2O(O_2CCH_2–C_{10}H_7)_2(Tp)_2$ (**10**), and $Fe_2O((O_2CCH_2CH_2)_2–C_{10}H_6)(Tp)_2$ (**11**) (where tren is tris(2-aminoethyl)amine, TPA is tris(2-pyridyl)amine, and Tp is hydrotrispyrazolylborate) have been characterized in terms of their structural, spectroscopic, magnetic, and photophysical properties. All four complexes exhibit moderately strong intramolecular antiferromagnetic exchange between the high-spin ferric ions (ca. -130 cm^{-1} for $\mathbf{H} = -2J\mathbf{S}_1\cdot\mathbf{S}_2$). Room-temperature steady-state emission spectra for compounds **8**–**11** in deoxygenated CH_3CN solution reveal spectral profiles similar to methyl-2-naphthyl acetate and $[Zn_2(OH)(O_2CCH_2–C_{10}H_7)_2(TACN\text{-}Me_3)_2](ClO_4)$ (**13**, where TACN-Me$_3$ is *N*,*N*,*N*-1,4,7-trimethyltriazacyclononane) but are significantly weaker in intensity relative to these latter two compounds. Time-resolved emission data for the iron complexes following excitation at 280 nm can be fit to simple exponential decay models with $\tau_{obs}^{S_1} = 36 \pm 2$, 32 ± 4, 30 ± 5, and 39 ± 3 ns for compounds **8**–**11**, respectively. The decays are assigned to the $S_1 \rightarrow S_0$ fluorescence of naphthalene; all of the lifetimes are less than that of the zinc model complex ($\tau_{obs}^{S_1} = 45 \pm 2$ ns), indicating quenching of the S_1 state by the iron–oxo core. Nanosecond time-resolved absorption data on $[Zn_2(OH)(O_2CCH_2–C_{10}H_7)_2(TACN\text{-}Me_3)_2](ClO_4)$ reveal a feature at $\lambda_{max} = 420$ nm that can be assigned as the $T_1 \rightarrow T_n$ absorption of the naphthalene triplet; the rise time of 50 ± 10 ns corresponds to an intersystem crossing rate of 2×10^7 s^{-1}. A similar feature (though much weaker in intensity) is also observed for compound **8**. The order-of-magnitude reduction in the T_1 lifetime of the pendant naphthalene for all of the iron–oxo complexes ($\tau_{obs}^{T_1} = 5 \pm 2$ μs vs 90 ± 10 μs for $[Zn_2(OH)(O_2CCH_2–C_{10}H_7)_2(TACN\text{-}Me_3)_2](ClO_4)$) indicates quenching of the naphthalene triplet with an efficiency of >90%. Neither the naphthalene radical cation nor the reduced $Fe^{II}Fe^{III}$ species were observed by transient absorption spectroscopy, implying that energy transfer is the most likely origin for the quenching of both the S_1 and T_1 states. Spectral overlap considerations strongly support a Förster (i.e., dipolar) mechanism for energy transfer from the S_1 state, whereas the lack of phosphorescence from either the free naphthyl ester or the Zn model complex suggests Dexter transfer to the diiron(III) core as the principal mechanism of triplet quenching. The notion of whether spin exchange within the diiron(III) core is in part responsible for the unusual ability of the iron–oxo core to engage in energy transfer from both the singlet and triplet manifolds of naphthalene is discussed.

Introduction

Electron exchange interactions play an important role in defining the electronic structure of systems composed of multiple, interacting paramagnetic centers. Manipulation of this interaction is at the heart of the field of molecular magnetic materials.[1−3] In addition, electron exchange coupling is manifested in a wide range of bioinorganic systems such as iron−sulfur clusters, non-heme iron−oxo proteins, and other important metal-containing cofactors.[4,5] Although the basic phenomenology of electron exchange has been

* To whom correspondence should be addressed. E-mail:jkm@cem.msu.edu.

(1) Kahn, O. *Acc. Chem. Res.* **2000**, *33*, 1.
(2) Kahn, O.; Martinez, C. J. *Science* **1998**, *279*, 44.
(3) Beltran, L. M. C.; Long, J. R. *Acc. Chem. Res.* **2005**, *38*, 325, and references therein.
(4) Lippard, S. J.; Berg, J. M. *Principles of Bioinorganic Chemistry*; University Science Books: Mill Valley, CA, 1994.
(5) Holm, R. H.; Kennepohl, P.; Solomon, E. *Chem. Rev.* **1996**, *96*, 2239−2314.

10.1021/ic0506761 CCC: $30.25
Published on Web 09/30/2005

thoroughly investigated (particularly in biological context[6−11]), there has been very little experimental work directed toward understanding its impact on the chemical reactivity of the molecules subject to this interaction.[12,13] We have therefore sought to develop chemical systems that will enable us to explore the interplay between electron exchange and electron and/or energy transfer chemistry in order to understand the role of intramolecular zero-field spin polarization in the reactivity of transition metal complexes.

Our initial efforts along these lines focused on photoinduced bimolecular reactions involving iron−oxo clusters.[13] This work allowed us to gain important insights into the methodology necessary for independently controlling factors such as driving force, reorganization energy, and electron exchange. Although a correlation between changes in reactivity and changes in the magnitude of intramolecular spin exchange within the clusters was implied from these studies, diffusion-limited reaction rates prevented us from drawing any definitive conclusions along these lines. Accordingly, we recently reported our first example of an intramolecular assembly where the donor and exchange-coupled cluster were covalently linked.[14] Photoexcitation of the naphthyl group in $[Fe_2O(O_2CCH_2-C_{10}H_7)_2(TACN\text{-}Me_3)_2](PF_6)_2$ (where TACN-Me_3 is *N*,*N*,*N*-1,4,7-trimethyltriazacyclononane) results in the formation of its singlet excited state, which can then react via energy or electron transfer with the spin-coupled diiron(III) core. The excited-state dynamics of this system were complicated by unexpected photophysical behavior resulting from an intramolecular excimer that formed between the two bridging naphthyl acetate groups. New systems were therefore sought which retained many of the desirable features of this assembly but precluded the formation of a naphthalene excimer so that a more thorough investigation of the photophysics of this type of donor−acceptor system could be carried out.

Herein we report the synthesis, structure, physical, and photophysical properties of a series of new diiron(III) complexes appended with bridging naphthalene groups. Three of the four complexes contain only a single naphthalene donor, thereby ensuring that intramolecular excimer formation cannot occur. The fourth complex—$Fe_2O(O_2CCH_2-C_{10}H_7)_2(Tp)_2$—employs the less sterically demanding tris(pyrazolyl)borate (Tp) capping ligand and likewise shows no evidence of excimer formation. All four of these complexes reveal dramatic changes in the excited-state dynamics of the naphthalene moiety relative to what is observed for either the free naphthalene or a Zn-containing analogue of the ferric complexes. In particular, the data show that the diiron(III) complex is capable of acting as an energy transfer acceptor from both the singlet and triplet manifolds of naphthalene, an unusual property that we believe may be linked to spin coupling within the iron−oxo core.

Experimental Section

General. All reagents were obtained from commercial sources and used without further purification. The compounds tris(2-pyridylmethyl)amine (TPA), potassium trispyrazolyl borate (KTp), and $[Fe_2OCl_6](NEt_4)_2$ were prepared according to literature procedures.[15,16] Elemental analyses and mass spectra were obtained through the analytical facilities at Michigan State University. ^{1}H NMR and ^{13}C NMR spectra were recorded on a Varian INOVA 300 MHz spectrometer.

1,3-Dimethylbromonaphthalene (1). The synthesis of this compound was based on methods already developed in the literature.[17] Under an argon atmosphere, a solution of 1.00 g (6.40 mmol) of 1,3-dimethylnaphthalene and 2.28 g (12.8 mmol) of *N*-bromosuccinimide in 10 mL of dry $CHCl_3$ was brought to reflux, then a small quantity of AIBN (∼10 mg) was added. The reaction was maintained at reflux for 12 h. It was cooled to room temperature, filtered, and the solvent was removed. Pure product was obtained by chromatographing on silica gel, eluting with hexanes. Yield: 1.02 g (51%). ^{1}H NMR ($CDCl_3$) δ: 8.13 (d, J_{Hz} = 6.3), 7.90 (d, J_{Hz} = 6.0), 7.84 (s), 7.59 (m), 4.95 (s), 4.65 (s). ^{13}C{^{1}H} NMR ($CDCl_3$) δ: 135, 134.2, 134.1, 131, 129, 128, 126, 125.5, 125, 124, 21.8, 19.4. Anal. Calcd for $C_{12}H_{10}Br_2$: C, 45.90; H, 3.21. Found: C, 45.10; H, 3.24.

1,3-Dimethylhydroxynaphthalene (2). The synthesis of this compound was based on methods already developed in the literature.[17] To 1.02 g (3.25 mmol) of **1** in 10 mL of 1,4-dioxane, 10 g (100 mmol) of $CaCO_3$ in 30 mL of H_2O was added. The resultant solution was brought to and maintained at reflux under an Ar atmosphere for 24 h. It was then cooled to room temperature, and the solvent was removed. The solids were extracted with CH_2Cl_2 (200 mL). The organic layer was dried over Na_2SO_4, and the solvent was removed. This crude alcohol was used without further purification. ^{1}H NMR ($CDCl_3$) δ: 7.85 (m), 7.67 (d, J_{Hz} = 3.0), 7.68 (d, J_{Hz} = 4.5), 7.52 (s), 7.41 (m), 7.35 (s), 4.88 (s), 4.58 (s), 3.64 (s).

Naphthalyl-1,3-dial (3). A solution of 200 mg (0.985 mmol) of **2** in 10 mL of dry CH_2Cl_2 was added dropwise to a rapidly stirring solution of pyridinium chlorochromate (425 mg, 1.97 mmol, in 5 mL of dry CH_2Cl_2). The resultant solution was stirred for 2 h. It was diluted with 5 equiv of diethyl ether and filtered. The solvent was removed, and the product was chromatographed on silica eluting with CH_2Cl_2/hexanes (1:1). Yield: 70 mg (40%). ^{1}H NMR ($CDCl_3$) δ: 10.44 (s), 10.24 (s), 9.32 (dd, J_{Hz} = 8.7, 0.9), 8.58 (s), 8.47 (s), 8.10 (td, J_{Hz} = 8.4, 0.6), 7.86 (dt, J_{Hz} = 7.2, 1.5), 7.72 (dt, J_{Hz} = 6.9, 1.2). ^{13}C{^{1}H} NMR ($CDCl_3$) δ: 193, 191, 140, 134, 133.5, 133, 132.5, 132, 130, 128, 126. MS [EI, *m*/*z* (rel int.)]: 184 (50) $[M]^+$, 155 (55) $[M - HCO]^+$, 127 (55) $[M - 2HCO]^+$.

1,3-Di(pro-2-eneoic acid)naphthalene (4). A solution of 630 mg (3.42 mmol) of **3** and 713 mg (6.85 mmol) of malonic acid in 5.0 mL of anhydrous pyridine was degassed. It was then treated with 1.00 mL (10.0 mmol) of piperidine. The resultant solution

(6) Blondin, G.; Girerd, J.-J. *Chem. Rev.* **1990**, *90*, 1359.
(7) Bersuker, I. B.; Borshch, S. A. *Adv. Chem. Phys.* **1992**, 703.
(8) Achim, C.; Bominaar, E. L.; Munck, E. *J. Biol. Inorg. Chem.* **1998**, *3*, 126.
(9) Bominaar, E. L.; Achim, C.; Borshch, S. A. *J. Chem. Phys.* **1999**, *110*, 11411.
(10) Bertrand, P.; Gayda, J.-P. *Biochim. Biophys. Acta* **1982**, *680*, 331.
(11) Mouesca, J. M.; Chen, J.-P.; Noodleman, L.; Bashford, D.; Case, D. A. *J. Am. Chem. Soc.* **1994**, *116*, 11898.
(12) Monzyk, M. M.; Holwerda, R. A. *Inorg. Chem.* **1992**, *31*, 1969−1971.
(13) Weldon, B. T.; Wheeler, D. E.; Kirby, J. P.; McCusker, J. K. *Inorg. Chem.* **2001**, *40*, 6802−6812.
(14) Picraux, L. B.; Weldon, B. T.; McCusker, J. K. *Inorg. Chem.* **2003**, *42*, 273−282.
(15) Trofimenko, S. *Inorg. Synth.* **1970**, *12*, 99−109.
(16) Armstrong, W. H.; Lippard, S. J. *Inorg. Chem.* **1985**, *24*, 981.
(17) Smith, J. G.; Dibble, P. W.; Sandborn, R. E. *J. Org. Chem.* **1986**, *51*, 3762.

was brought to and maintained at reflux for 6 h, cooled to room temperature, and poured onto acidic ice. The yellow precipitate was collected by filtration and washed with water. The crude product was used without further purification. ^{1}H NMR (CD_3OD) δ: 8.51 (d, $J_{Hz} = 15.6$), 8.19 (d, $J_{Hz} = 7.8$), 8.14 (s), 8.10 (s), 8.00 (d, $J_{Hz} = 18.9$), 7.66 (dt, $J_{Hz} = 6.9, 1.5$), 7.60 (d, $J_{Hz} = 6.6, 1.5$), 6.72 (d, $J_{Hz} = 15.9$), 6.68 (d, $J_{Hz} = 15.9$).

1,3-Di(methyl-3-pro-2-eneoate)naphthylene (5). The crude acid **4** was dissolved in 50 mL of methanol, and 0.5 mL of concentrated HCl was added. The reaction mixture was brought to and maintained at reflux for 24 h under an Ar atmosphere. The reaction mixture was cooled, and the methanol was removed. The crude product was dissolved in H_2O and extracted into CH_2Cl_2 (3 × 40 mL). The pure product was obtained by chromatographing on silica, eluting with hexanes/CH_2Cl_2 (1:1). Yield: 700 mg (68%). ^{1}H NMR ($CDCl_3$) δ: 8.49 (d, $J_{Hz} = 15.9$), 8.16 (d, $J_{Hz} = 7.8$), 7.98 (s), 7.90 (d, $J_{Hz} = 8.7$), 7.83 (s), 7.63 (t, $J_{Hz} = 7.8$), 7.58 (t, $J_{Hz} = 6.9$), 6.60 (d, $J_{Hz} = 15.9$), 6.58 (d, $J_{Hz} = 15.9$), 3.89 (s), 3.86 (s). ^{13}C{^{1}H} NMR ($CDCl_3$) δ: 167.5, 167, 144, 142, 134, 133, 132.5, 132, 131.5, 130, 128, 127, 124, 123, 122, 119, 52.2, 52.1.

1,3-Di(methyl-3-propionate)naphthalene (6). A solution of 100 mg (0.338 mmol) of **5** and 10 mg of Pd/C in 50 mL of ethanol was bubbled with H_2 for 15 h. The solution was filtered through Celite, and the solvent was removed to produce a pale yellow oil. Analytically pure product was obtained by chromatographing on silica, eluting with 100% hexanes. Yield: 100 mg (99%). ^{1}H NMR ($CDCl_3$) δ: 7.98 (d, $J_{Hz} = 8.4$), 7.82 (d, $J_{Hz} = 9.3$), 7.55 (s), 7.49 (t, $J_{Hz} = 3.9$), 7.23 (s), 3.72 (s), 3.70 (s), 3.41 (t, $J_{Hz} = 8.1$), 3.10 (t, $J_{Hz} = 7.8$), 2.76 (m). ^{13}C{^{1}H} NMR ($CDCl_3$) δ: 173.7, 173.6, 138, 137, 134, 131, 129, 127, 126, 125.9, 123, 52.0, 35.8, 35.3, 31.2, 28.4. Anal. Calcd for $C_{18}H_{20}O_4$: C, 71.98; H, 6.71. Found: C, 72.17; H, 6.10. Electronic absorption spectrum in CH_3CN at 298 K [λ_{max}, nm (ϵ, M^{-1} cm^{-1})]: 280 (10 000).

1,3-Di(propionic acid)naphthalene (7). Under an argon atmosphere, 500 mg (1.67 mmol) of **6** and 187 mg (3.33 mmol) of KOH in 20 mL of H_2O were brought to and maintained at reflux for 3 h. The solution was then cooled to room temperature and brought to pH 2 with dilute HCl(aq). The product was extracted into 60 mL of CH_2Cl_2. This organic layer was washed (2 × 20 mL) with H_2O and dried over Na_2SO_4. The solvent was removed, and analytically pure product was obtained by recrystallization from H_2O as a pale yellow solid. Yield: 450 mg (90%). ^{1}H NMR ($CDCl_3$) δ: 7.89 (d, $J_{Hz} = 8.4$), 7.64 (d, $J_{Hz} = 9.6$), 7.39 (s), 7.32 (t, $J_{Hz} = 3.8$), 7.11 (s), 3.25 (t, $J_{Hz} = 7.5$), 2.92 (t, $J_{Hz} = 7.5$), 2.64 (t, $J_{Hz} = 7.5$), 2.56 (t, $J_{Hz} = 7.5$). Anal. Calcd for $C_{16}H_{16}O_4 \cdot 1/2H_2O$: C, 68.32; H, 5.73. Found: C, 68.28; H, 5.41.

[$Fe_2O(O_2CCH_2-C_{10}H_7)(tren)_2$]($BPh_4$)($NO_3$)$_2$ (8). Under a dinitrogen atmosphere, a solution of $Fe(NO_3)_3 \cdot 9H_2O$ (323 mg, 0.800 mmol) in 30 mL of methanol was added dropwise to a rapidly stirring solution of tren (117 mg, 0.800 mmol) in 30 mL of methanol, resulting in a yellow-brown solution. To this solution, 74 mg (0.40 mmol) of 2-naphthylacetic acid and 40 mg (0.40 mmol) of NEt_3 in 10 mL of methanol were added. The solution became cloudy and was filtered. To the filtrate, 1.23 g (3.6 mmol) of $NaBPh_4$ in 10 mL of methanol was added. The resulting solution was stirred briefly and then allowed to stand overnight. Green-brown block-shaped crystals were filtered and washed with methanol (3 × 20 mL) and diethyl ether (10 mL). The product was then dried under vacuum. A crystal suitable for X-ray diffraction studies was obtained from this sample. Yield: 271 mg (30%). Anal. Calcd for $C_{48}H_{65}N_{10}BFe_2O_9 \cdot 2CH_3OH \cdot H_2O$: C, 53.1; H, 6.7; N, 12.4. Found: C, 52.8; H, 6.5; N, 12.7. Electronic absorption spectrum in CH_3CN at 298 K [λ_{max}, nm (ϵ, M^{-1} cm^{-1})]: 700 (300), 490 (800), 460 (1000), 320 (9900), 270 (11 500).

[$Fe_2O(O_2CCH_2-C_{10}H_7)(TPA)_2$]($ClO_4$)$_3$ (9). The synthesis of this compound was based on methods already developed in the literature.[18] A solution of 289 mg (0.219 mmol) of TPA·4ClO_4 and 169 mg (1.68 mmol) of NEt_3 in 20 mL of methanol was added dropwise to a rapidly stirring solution of 226 mg (0.419 mmol) of $Fe(ClO_4)_3$ in 1 mL of methanol. To the resultant mixture, 39 mg (0.21 mmol) of 2-naphthylacetic acid and 21 mg (0.21 mmol) of NEt_3 in 1 mL of methanol was added. The solution was stirred briefly and then allowed to stand for 1 h. The precipitate was filtered and washed with 1 mL of methanol and 20 mL of diethyl ether. The product was dried under vacuum to obtain analytically pure product. X-ray quality crystals were obtained as green-brown plates from slow evaporation of a CH_3CN solution of the compound at room temperature. Yield: 300 mg (60%). MS [FAB^+, *m*/*z* (rel int.)]: 1091 (25) [M − ClO_4]$^+$, 992 (20) [M − 2ClO_4]$^+$. Anal. Calcd for $C_{48}H_{45}N_8Cl_3Fe_2O_{15}$: C, 48.37; H, 3.81; N, 9.40. Found: C, 47.70; H, 3.96; N, 9.39. Electronic absorption spectrum in CH_3CN at 298 K [λ_{max}, nm (ϵ, M^{-1} cm^{-1})]: 700 (100), 500 (2000), 460 (3000), 320 (7000), 260 (18 000).

$Fe_2O(O_2CCH_2-C_{10}H_7)_2(Tp)_2$ (10). The synthesis of this compound was based on methods already developed in the literature.[20] A rapidly stirring solution of 161 mg (0.269 mmol) of [Fe_2OCl_6]-(NEt_4)$_2$ in 10 mL of CH_3CN was treated with 100 mg (0.538 mmol) of 2-naphthylacetic acid and 109 mg (0.538 mmol) of NEt_3 in 3 mL of CH_3CN. The solution was stirred for 10 min, and then 122 mg (0.484 mmol) of KTp in 15 mL of CH_3CN was added over 5 min. The resultant solution was allowed to stir for an additional 20 min, then filtered. The solvent was removed, and the product was taken up in 15 mL of diethyl ether. This solution was filtered, and the precipitate was washed with 20 mL of diethyl ether. The solvent was removed, and the product was dissolved in minimal CH_2Cl_2 (∼2 mL). To this solution was added 4 vol. equiv. of hexanes. This resultant solution was put under a slow stream of nitrogen until a green-brown precipitate was evident. The solid was collected and dried under vacuum to afford pure product. X-ray quality, green-brown plates were grown from slow evaporation of a CH_3-CN solution of the compound at −10 °C. Yield: 100 mg (22%). MS [FAB^+, *m*/*z* (rel int.)]: 925 (3) [MH]$^+$. Anal. Calcd for $C_{42}H_{38}N_{12}B_2Fe_2O_5 \cdot OEt_2$: C, 55.35; H, 4.85; N, 16.84. Found: C, 56.01; H, 4.67; N, 17.02. Electronic absorption spectrum in CH_3-CN at 298 K [λ_{max}, nm (ϵ, M^{-1} cm^{-1})]: 700 (100), 500 (1000), 460 (1000), 340 (12 000), 270 (23 000).

$Fe_2O((O_2CCH_2CH_2)_2-C_{10}H_6)(Tp)_2$ (11). The synthesis of this compound was based on a previously published procedure.[19] A solution of 146 mg (0.538 mmol) of **7** and 109 mg (1.08 mmol) of NEt_3 in 10 mL of CH_3CN was added dropwise to a rapidly stirring solution of 323 mg (0.538 mmol) of [Fe_2OCl_6](NEt_4)$_2$ in 10 mL of CH_3CN. The solution was stirred for 20 min and then brought to a boil for ∼1 min. The reaction was allowed to slowly cool to room temperature, then treated with 190 mg (0.753 mmol) of KTp in 25 mL of CH_3CN over 5 min. The resultant mixture was stirred for an addition 20 min, then filtered. The solvent was removed, and a portion of the solid was dissolved in 5 mL of CH_2Cl_2. To this solution was added 5 mL of hexanes, and a red solid (assumed to be [$Fe(Tp)_2$]Cl)[19] was filtered from the solution. The solution was placed under a gentle stream of nitrogen. It was filtered frequently to remove additional [$FeTp_2$]Cl that continued to

(18) Norman, R. E.; Holz, R. C.; Menage, S.; O'Conner, C. J.; Zhang, J. H.; Que, L. *Inorg. Chem.* **1990**, *29*, 4629−4637.
(19) Armstrong, W. H.; Spool, A.; Papaefthymiou, G. C.; Frankel, R. B.; Lippard, S. J. *J. Am. Chem. Soc.* **1984**, *106*, 3653−3667.

Table 1. Crystallographic Data for $[Fe_2O(O_2CCH_2-C_{10}H_7)(tren)_2](BPh_4)(NO_3)_2$ (**8**), $[Fe_2O(O_2CCH_2-C_{10}H_7)(TPA)_2](ClO_4)_3$ (**9**), and $Fe_2O(O_2CCH_2-C_{10}H_7)_2(Tp)_2$ (**10**)

	8	**9**	**10**
mol formula	$C_{50}H_{65}N_{10}Fe_2BO_{11}$	$C_{48}H_{45}N_8Cl_3Fe_2O_{16}$	$C_{46}H_{44}N_{14}Fe_2B_2O_5$
mol wt	1104.63	1207.97	1006.27
cryst color, habit	green-brown, blocks	green-brown, plates	green-brown, plates
cryst system	triclinic	orthorhombic	orthorhombic
space group	*P*1	$Pna2_1$	*Pnma*
T/K	173 (2)	173 (2)	173(2)
a/Å	10.230(1)	22.489(5)	15.412(3)
b/Å	15.775(2)	22.414(5)	23.799(5)
c/Å	18.864(2)	10.422(2)	13.060(3)
α/°	69.26	90.00	90.00
β/°	77.29	90.00	90.00
γ/°	73.25	90.00	90.00
V/Å^3	2702.4(5)	5253.2(2)	4790.3(2)
Z	2	4	4
D_{calcd} (g cm^{-1})	1.358	1.527	1.395
GOF (F^2)	0.911	1.058	0.941
R_1[a]	0.069	0.048	0.040
wR_2[b]	0.078	0.124	0.073

[a] $R_1 = \sum||F_o| - |F_c||/\sum|F_o|$. [b] $wR_2 = [\sum w(F_o^2 - F_c^2)^2/\sum w(F_o^2)^2]^{1/2}$, $w = 1/[\sigma^2(F_o^2) + (aP)^2 + bP]$, where $P = [F_o^2 + 2F_c^2]/3$.

precipitate. When most of the solution had been evaporated, an orange-brown precipitate was collected. The precipitate was recrystallized from 1 mL of CH_2Cl_2 and 4 mL of hexanes by placing it under a gentle stream of nitrogen. Yield: 70 mg (18%). MS [FAB$^+$, *m*/*z* (rel int.)]: 825 (6) $[MH]^+$. Anal. Calcd for $C_{34}H_{35}N_{12}B_2Fe_2O_5 \cdot C_6H_{14}$: C, 52.80; H, 5.43; N, 20.01. Found: C, 52.61; H, 5.32; N, 19.86. Electronic absorption spectrum in CH_3CN at 298 K [λ_{max}, nm (ϵ, M^{-1} cm^{-1})]: 710 (100), 500 (1000), 460 (1500), 350 (11 000).

Methyl-2-Naphthyl Acetate (12). This compound was synthesized according to literature procedures.[14] ^1H NMR ($CDCl_3$): δ 7.85−7.81 (m, 3 H), 7.75 (s, 1 H), 7.50−7.42 (m, 3 H), 3.82 (s, 2 H), 3.73 (s, 3 H). $^{13}C\{^1H\}$ NMR ($CDCl_3$): δ 176.9, 133.7, 132.8, 131.7, 128.5, 128.2, 127.9, 127.6, 126.4, 126.1, 52.4, 41.6. Anal. Calcd for $C_{13}H_{12}O_2$: C, 77.98; H, 6.04. Found: C, 77.99; H, 6.22. Electronic absorption spectrum in CH_3CN at 298 K [λ_{max}, nm (ϵ, M^{-1} cm^{-1})]: 268 (4820), 276 (5090), 286 (3410).

$[Zn_2(OH)(O_2CCH_2-C_{10}H_7)_2(TACN\text{-}Me_3)_2](ClO_4)$ (13). This compound was synthesized by a method previously described in the literature.[14] ^1H NMR ($CDCl_3$): δ 7.88−7.80 (m, 6 H), 7.72 (s, 2 H), 7.51−7.41 (m, 6 H), 3.68 (s, 4 H), 2.62−2.44 (m, 19 H), 2.39−2.29 (m, 23 H), 2.22 (s, 9 H). Anal. Calcd for $C_{42}H_{61}N_6O_9Zn_2Cl$: C, 52.54; H, 6.40; N, 8.75. Found: C, 52.52; H, 6.02; N, 8.63. MS (FAB): *m*/*z* 860 ($[M - ClO_4]^+$). Electronic absorption spectrum in CH_3CN at 298 K [λ_{max}, nm (ϵ, M^{-1} cm^{-1})]: 278 (1650), 284 (1700), 292 (1100).

Physical Measurements: X-ray Structure Determinations. Single-crystal X-ray diffraction data for $[Fe_2O(O_2CCH_2-C_{10}H_7)(tren)_2](BPh_4)(NO_3)_2$ (**8**), $[Fe_2O(O_2CCH_2-C_{10}H_7)(TPA)_2](ClO_4)_3$ (**9**), and $Fe_2O(O_2CCH_2-C_{10}H_7)_2(Tp)_2$ (**10**) were collected on a Siemens SMART diffractometer equipped with an Oxford Cryosystems low-temperature device at the X-ray facility of Michigan State University. Crystallographic data are summarized in Table 1. Lattice parameters were obtained from least-squares analyses. Crystals showed no significant decay during the data collection. Data were integrated (SAINT),[20] corrected for Lorentz and polarization effects, and analyzed for agreement and possible absorption (SADABS) using XPREP.[21] Space group assignments were based on systematic absences, packing considerations, a statistical analysis of intensity distribution, and successful refinement of the structure. The structures were solved by direct methods and expanded using Fourier techniques. All structure calculations were performed with the SHELXTL 5.1 software package.[21] All non-hydrogen atoms were refined anisotropically. The hydrogen atoms were located in the difference electron density map and refined accordingly. Further details concerning the structure determinations may be found in Supporting Information.

Cyclic Voltammetry. Electrochemical measurements were carried out in a N_2-filled drybox (Vacuum Atmospheres) using a BAS CV-50W electrochemical analyzer. A standard three-electrode configuration was employed consisting of Pt working and counter electrodes and a $Ag/AgNO_3$ reference electrode. Compounds were dissolved in CH_3CN that was 0.1 M in NBu_4PF_6; the CH_3CN had been passed over a silica column, distilled first from $KMnO_4$ then CaH_2, and degassed. Ferrocene was added to all solutions to provide for internal calibration.

Variable Temperature Magnetic Susceptibility. Magnetic susceptibility data were collected using a Quantum Design MPMS SQUID magnetometer interfaced to an IBM PC. Data were collected in an applied field of 2 T. Following each temperature change, the system was kept at the new temperature for an additional 5 min before data collection to ensure thermal equilibration of the sample. Data were corrected for diamagnetism of the sample using Pascal's constants and for the measured susceptibility of the sample holder and are reported herein as effective magnetic moments. Data were fit to the van Vleck equation using Magfit.[22] Solution susceptibility measurements at room temperature were made via the Evan's NMR method using a Varian 300 MHz spectrometer.[23] The shift of the *tert*-butyl alcohol $-CH_3$ resonance in a 10% *tert*-butyl alcohol/CD_3CN solution relative to that of an internal standard was used to determine $\Delta\nu$.

Electronic Absorption and Steady-State Emission Measurements. All spectroscopic data were obtained on samples in sealed cells and dissolved in CH_3CN that had been passed over a silica column, doubly distilled (from $KMnO_4$, then CaH_2), degassed, and stored under an inert atmosphere. Electronic absorption spectra were recorded using a Hewlett-Packard 8452A diode array spectrophotometer. Steady-state emission spectra were acquired using a Spex

(20) *SAINT*, 6.02 ed.; Bruker AXS: Madison, WI, 1999.
(21) *SHELXTL*, 5.1 ed.; Siemens Industrial Automation, Inc.: Madison, WI, 1995.
(22) Schmitt, E. Ph.D. Dissertation, Department of Chemistry, University of Illinois, Urbana-Champaign, IL, 1996.
(23) Schubert, E. M. *J. Chem. Educ.* **1992**, *69*, 62.

FluoroMax fluorimeter. Emission spectra were corrected for instrumental response by using a NIST standard of spectral irradiance (Optronic Laboratories, Inc., OL220M tungsten quartz lamp). All subsequent data manipulations were carried out with the corrected spectra as described elsewhere.[24]

Radiative quantum yields (Φ_r) were determined relative to triphenylene ($\Phi_r = 0.065$ in ethanol[25,26]) that had been purified by recrystallization from hexanes. Measurements were carried out on optically thin solutions (o.d. ~ 0.1). The samples were prepared in an Ar atmosphere drybox in 1 cm path length sealed quartz cuvettes. Quantum yields were calculated according to eq 1,

$$\Phi_{unk} = \Phi_{std}\frac{(I_{unk}/A_{unk})}{(I_{std}/A_{std})}\left(\frac{\eta_{unk}}{\eta_{std}}\right)^2 \quad (1)$$

where Φ_{unk} and Φ_{std} are the radiative quantum yields of the sample and the standard, I_{unk} and I_{std} are the integrated emission intensities of the sample and standard, A_{unk} and A_{std} are the absorbances of the sample and standard at the excitation wavelength (280 nm), and η_{unk} and η_{std} are the indices of refraction of the sample and standard solutions (taken to be equivalent to neat CH_3CN and EtOH), respectively. The excitation wavelength cited in the literature for the absolute quantum yield measurement of triphenylene is 254 nm;[25] however, at this wavelength the absorption spectrum of the diiron−naphthalene assembly is dominated by features associated with the iron−oxo core in contrast to their roughly equal contributions at $\lambda = 280$ nm. The excitation spectrum of triphenylene in EtOH was found to be in good agreement with the compound's absorption spectrum over the limited range of wavelengths examined (250−300 nm), implying that the emission quantum yield of triphenylene does not vary significantly with excitation wavelength in this spectral region. We therefore used the absolute value of Φ_r for triphenylene as reported at $\lambda_{ex} = 254$ nm[25] as our standard at $\lambda_{ex} = 280$ nm to determine relative values for the molecules described in this study.

Time-Correlated Single-Photon Counting Emission Spectroscopy (TCSPC). The apparatus used for acquisition of emission data via TCSPC is described elsewhere.[27] Briefly, a mode-locked Ar-ion laser was used to synchronously pump a dye laser charged with pyromethane 567. The 280 nm light used for excitation was obtained by doubling the 560 nm dye output in a KDP type I second harmonic crystal. The excitation beam was attenuated using neutral density filters as needed to ensure linear response. Samples (o.d. ~ 0.1) were sealed under Ar in 1 cm path length quartz cuvettes, and the emission was monitored at 350 nm (10 nm band-pass). Emission was detected at the magic angle (54.7°) relative to the excitation polarization to eliminate any effects due to anisotropy. The measured instrument response function (IRF) was ca. 30 ± 5 ps (fwhm); data were collected over 1064 channels corresponding to time windows of up to 200 ns, depending on the time constant for emission.

Lifetimes were determined by fitting the data to exponential decay models using the Microcal Origin 6.0 software package.[28] Due to the density of data points, data were fit for delay times $\Delta t \geq 1$ ns for a 200 ns window and $\Delta t \geq 0.5$ ns for a 50 ns window. In addition to the naphthalene-based emission, all compounds exhibited a weak emissive component with $\tau = 3 \pm 1$ ns. This component was traced to an impurity in the CH_3CN solvent that could not be completely eliminated despite multiple distillations. The contribution of this impurity was therefore incorporated as a fixed parameter into the fitting of all of the emission data reported herein.

Time-Resolved Electronic Absorption Spectroscopy. Nanosecond time-resolved absorption measurements were carried out using a Nd:YAG-based laser spectrometer that has been described previously.[24] The present system has been modified since this earlier report by the incorporation of a 2035 McPherson monochromator (replacing the Jarrel-Ashe Monospec 18) and inclusion of an Advanced Photonix Model 6208c avalanche photodiode (APD) operating at −12 V. Each sample was dissolved in CH_3CN (purified as stated above) with an absorbance of ~1 (1 cm path length) at the excitation wavelength of 266 nm and sealed under an Ar atmosphere in a quartz cuvette. The data correspond to a 90 shot average of the signal (acquired at 0.2 Hz) and baseline as well as background sample emission with 1.5 mJ of power at the sample; the baseline and emission were subsequently subtracted from the signal and the data analyzed using programs of local origin. The rise times of the absorbances at $\lambda_{probe} = 420$ nm were fit via iterative reconvolution of the measured IRF of the apparatus (fwhm $= 13 \pm 2$ ns) with a single-exponential kinetic model. All other data characterized by time constants much longer than the IRF were fit directly, i.e., no convolution was required. Absorption spectra acquired before and after data acquisition did not reveal any indication of significant sample decomposition over the course of the measurement. However, it should be noted that several of these compounds have been observed to decompose upon prolonged photolysis.

Results and Discussion

A. Structure and Basic Physical Properties of Naphthalene-Appended Dinuclear Iron−Oxo Complexes. In the present study, four complexes employing naphthalene as a donor and an exchange-coupled iron−oxo cluster as an acceptor were prepared using modified literature procedures.[18,19] $Fe_2O(O_2CCH_2{-}C_{10}H_7)_2(Tp)_2$ (**10**) is analogous to a donor−acceptor system that we have previously described[14] (i.e., a system containing two naphthyl acetate donors) in which TACN-Me_3 has been replaced with hydrotris(pyrazolyl)borate (Tp) as the capping ligand. This modification was done, in part, to determine if the excimer formation documented in the previous case[14] was associated with the steric constraints imposed by the TACN-Me_3 ligand. All of the remaining compounds described herein contain a single bridging naphthalene donor moiety, thus precluding intramolecular excimer formation entirely. This was achieved in complexes **8** and **9** by using tetradentate capping ligands (tren and TPA, respectively). Compound **11** still features the tridentate Tp ligand; however, the two carboxylates needed to complete the coordination sphere of the metal ions derive from a single naphthalene modified with two $-(CH_2CH_2{-}CO_2)-$ groups at the 1 and 3 positions (Scheme 1).

X-ray quality crystals were obtained for $[Fe_2O(O_2CCH_2{-}C_{10}H_7)(tren)_2](BPh_4)(NO_3)_2$ (**8**), $[Fe_2O(O_2CCH_2{-}C_{10}H_7)(TPA)_2](ClO_4)_3$ (**9**), and $Fe_2O(O_2CCH_2{-}C_{10}H_7)_2(Tp)_2$ (**10**);

(24) Damrauer, N. H.; Boussie, T. R.; Devenney, M.; McCusker, J. K. *J. Am. Chem. Soc.* **1997**, *119*, 8253−8268.
(25) Dawson, W. R.; Windsor, M. W. *J. Phys. Chem.* **1968**, *72*, 3251−3260.
(26) The ethanol was distilled over 4 Å molecular sieves and stored under an inert atmosphere prior to use.
(27) DeWitt, L.; Blanchard, G. J.; LeGoff, E.; Benz, M. E.; Liao, J. H.; Kanatzidis, M. G. *J. Am. Chem. Soc.* **1993**, *115*, 12158−12164.
(28) *Origin*, 6.0 ed.; Microcal Software, Inc.: Northampton, MA, 1991−1999.

Scheme 1

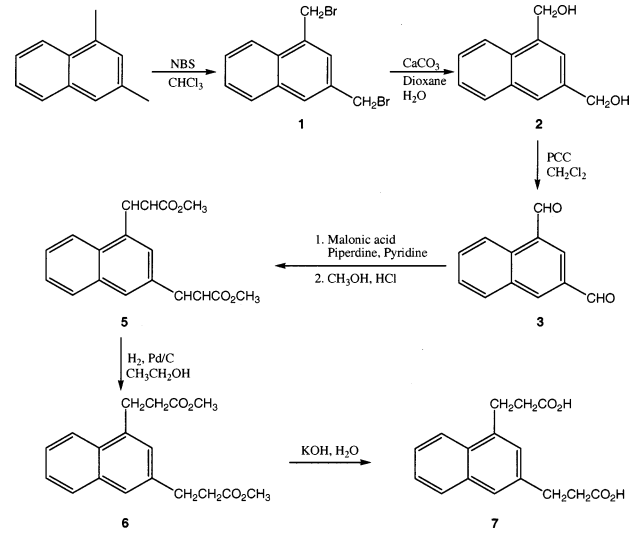

crystallographic details are given in Table 1. Drawings of **8**, **9**, and **10** are shown in Figures 1, 2, and 3, respectively. Selected bond lengths and angles for all three complexes are listed in Table 2. The metric details for these compounds are largely unremarkable and similar to those reported for this class of molecules. For example, the average Fe−O_{bridge} bond length for **8**, **9**, and **10** is ∼1.79 Å: this can be compared to values found for $[Fe_2O(O_2C-C_6H_5)_2(TPA)_2](ClO_4)_3$ (1.790 Å)[18] and $Fe_2O(O_2CCH_3)_2(Tp)_2$ (1.784 Å).[19] Likewise, the average Fe−O−Fe bond angle of 130 ± 5° is well within the range found for related complexes such as $[Fe_2O(O_2C-C_6H_5)_2(TPA)_2](ClO_4)_3$ (130.0(2)°) and $Fe_2O(O_2CCH_3)_2(Tp)_2$ (124.9(2)°).[18,19] In compound **9**, the bridging 2-naphthlyacetate is asymmetrically bonded to the two iron centers with bond lengths of 1.961(4) and 2.034(4) Å, similar to $[Fe_2O(O_2C-C_6H_5)_2(TPA)_2](ClO_4)_3$ whose Fe−O(carboxylate) bond distances are 1.984(5) and 2.046(5) Å.[18] More symmetric ligation is found for both **8** and **10**, with the 2-naphthlacetate groups exhibiting Fe−O bond lengths of 2.04(1) Å and 2.047(5) Å, respectively. The metric details within the naphthalene rings are as expected with average C−C bond distances of 1.40 Å for each complex; deviations from planarity are minimal in all three structures. No

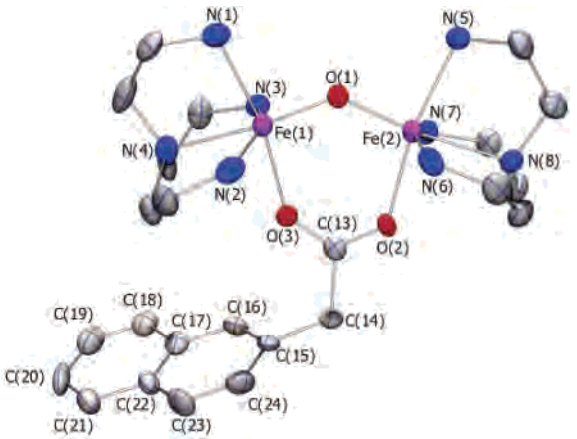

Figure 1. Drawing of the cation of $[Fe_2O(O_2CCH_2C_{10}H_7)(tren)_2](BPh_4)(NO_3)_2$ (**8**) obtained from a single-crystal X-ray structure determination. Atoms are represented as 50% probability thermal ellipsoids.

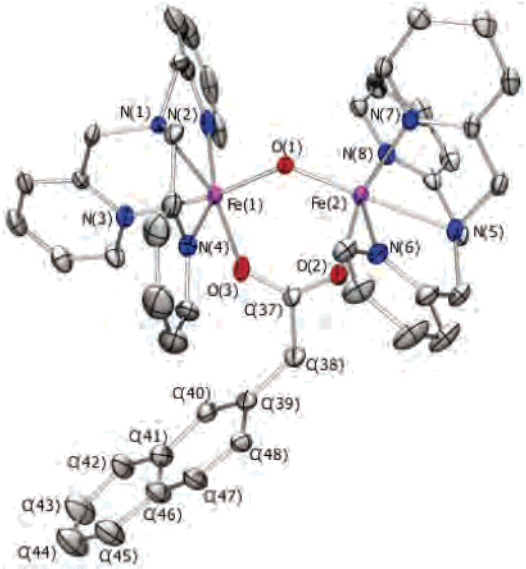

Figure 2. Drawing of the cation of $[Fe_2O(O_2CCH_2C_{10}H_7)(TPA)_2](ClO_4)_3$ (**9**) obtained from a single-crystal X-ray structure determination. Atoms are represented as 50% probability thermal ellipsoids.

significant intramolecular interactions between the two bridging naphthyl acetate groups are evident for complex **10**, in stark contrast to what was observed for the TACN-Me_3 analogue. This along with spectroscopic data to be described later supports our earlier suggestion that excimer formation in $[Fe_2O(O_2CCH_2-C_{10}H_7)_2(TACN\text{-}Me_3)_2]^{2+}$ was driven in large part by steric constraints stemming from the TACN-Me_3 ligands.[14] Intramolecular interactions are less of a concern for complexes **8** and **9**. Nevertheless, no unusual contacts are apparent. There does appear to be some interaction between naphthyl groups of adjacent cations in complex **9**, but there is no evidence to suggest that this interaction is retained in solution.

Unfortunately, we were unable to grow X-ray quality crystals for $Fe_2O((O_2CCH_2CH_2)_2-C_{10}H_6)(Tp)_2$ (**11**). All crystallization conditions employed produced oils, powders, or very thin plates that did not diffract sufficiently to allow for refinement. Efforts to obtain more suitable crystals are still underway.

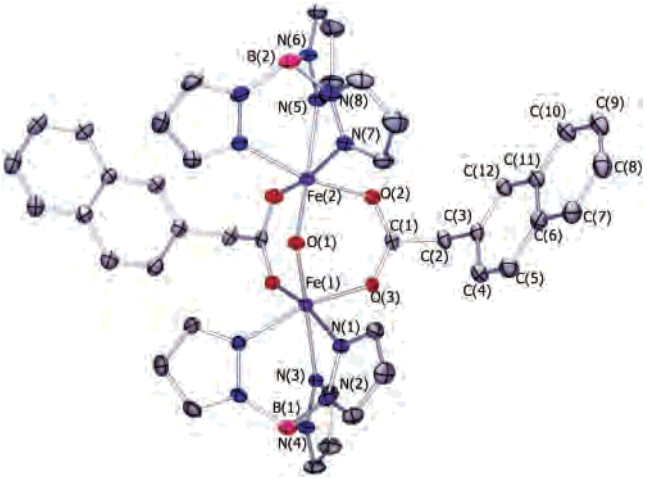

Figure 3. Drawing of $Fe_2O(O_2CCH_2C_{10}H_7)_2(Tp)_2$ (**10**) obtained from a single-crystal X-ray structure determination. Atoms are represented as 50% probability thermal ellipsoids.

Table 2. Selected Bond Distances (Å) and Angles (deg) for $[Fe_2O(O_2CCH_2{-}C_{10}H_7)(tren)_2](BPh_4)(NO_3)_2$ (**8**), $[Fe_2O(O_2CCH_2{-}C_{10}H_7)(TPA)_2]$ $(ClO_4)_3$ (**9**), and $Fe_2O(O_2CCH_2{-}C_{10}H_7)_2(Tp)_2$ (**10**)

	8	9	10
Bond Distances (Å)			
Fe(1)−O(1)	1.773(3)	1.803(4)	1.785(3)
Fe(2)−O(1)	1.790(3)	1.788(4)	1.787(3)
Fe(1)−O(3)	2.036(4)	1.961(4)	2.052(2)
Fe(2)−O(2)	2.054(3)	2.034(4)	2.043(3)
Fe(1)−N(1)	2.149(4)	2.181(5)	2.164(3)
Fe(1)−N(2)	2.179(4)	2.130(6)	*a*
Fe(1)−N(3)	2.149(4)	2.216(5)	2.200(4)
Fe(1)−N(4)	2.238(4)	2.142(5)	*a*
Fe(2)−N(5)	2.147(4)	2.236(5)	2.180(4)
Fe(2)−N(6)	2.150(4)	2.124(5)	*a*
Fe(2)−N(7)	2.162(4)	2.118(5)	2.151(3)
Fe(2)−N(8)	2.266(4)	2.144(5)	*a*
Fe(1)···Fe(2)	3.28	3.26	3.17
C_{Nap}−Fe(1)Fe(2)[b]	4.8	4.8	4.7
centroid−O(1)[c]	7.1	7.5	6.5
Bond Angles (deg)			
Fe(1)−O(1)−Fe(2)	134.4(2)	130.0(2)	124.9(2)
O(1)−Fe(1)−O(3)	96.3(2)	101.7(2)	96.2(1)
O(1)−Fe(2)−O(2)	99.1(1)	98.6(2)	96.5(1)

[a] In compound **10**, the atoms N(2), N(4), N(6), and N(8) are the nitrogens in the pyrazole rings which are bound to the boron atoms of the Tp capping ligand. Only the unique atoms are listed here (i.e., the symmetry equivalent bond lengths have been omitted). [b] The C_{Nap} refers to the C atom of the naphthalene ring to which the acetate group is attached (C(15) in **8**, C(39) in **9**, and C(3) in **10**); Fe(1)Fe(2) refers to the midpoint of the Fe(1)···Fe(2) vector. [c] The centroid refers to the center of the naphthalene ring (midpoint of C(17)−C(22) in **8**, C(41)−C(46) in **9**, and C(6)−C(11) in **10**).

A.1. Electrochemistry. The electrochemical properties of all four complexes were examined using cyclic voltammetry; the data are summarized in Table 3. It should be noted that most of the observed features were irreversible or at best quasi-reversible. However, this is not uncommon for this class of compounds.[14,16,19] The potentials we quote in these instances therefore correspond to peak potentials as opposed to $E_{1/2}$ values. Assignments were based largely upon comparison with data acquired for $C_{10}H_7CH_2CO_2CH_3$ (**12**), $C_{10}H_6(CH_2CH_2CO_2CH_3)_2$ (**6**), and $[Zn_2(OH)(O_2CCH_2{-}C_{10}H_7)_2(TACN\text{-}Me_3)_2](ClO_4)$ (**13**). Compound **8** shows two irreversible reductions at −0.60 and −1.78 V, as well as an irreversible oxidation at +1.46 V. The latter two signals can be immediately ascribed to the reduction and oxidation, respectively, of the naphthalene moiety based on the nearly identical values obtained for the Zn complex (Table 3). The feature at −0.60 V can therefore be assigned as the $Fe^{III} \rightarrow Fe^{II}$ reduction.

The other three compounds—all of which contain aromatic capping ligands—show somewhat more complicated electrochemical behavior. Compound **10** shows two quasi-reversible reductions at −1.07 and −2.05 V. The signal at −1.07 V can be assigned to the $Fe^{III} \rightarrow Fe^{II}$ reduction based on the value of −1.04 V reported in the closely related complex $Fe_2O(O_2CCH_3)_2(Tp)_2$.[19,29] The feature at −2.05 V is therefore assigned to the formation of the naphthalene radical anion. The origin of the significant shift in both of these potentials relative to those of complex **8** is not entirely clear. One possibility is that the negative shift in the reduction potential of the metal upon replacing tren with the more electron rich Tp ligand is influencing the potential of the naphthyl group via the bridging carboxylate. Two irreversible oxidations are also observed for compound **10**, one at +1.3 V and another at +1.6 V. One of these certainly corresponds to oxidation of the naphthalene group; the other likely represents oxidation of the Tp ligand. Unfortunately, given how close both of these values are to the +1.5 V potential observed for oxidation of naphthalene in $[Zn_2(OH)(O_2CCH_2{-}C_{10}H_7)_2(TACN\text{-}Me_3)_2]^+$, a more specific assignment is not possible at the present time. The electrochemistry of complex **11** showed one irreversible reduction at −1.1 V ($Fe^{III} \rightarrow Fe^{II}$) and two irreversible oxidations at +1.4 V (naphthalene oxidation) and +1.8 V. Given the qualitative similarity between the electrochemical behavior of complexes **10** and **11**, this second oxidation is tentatively ascribed to the Tp ligand.

Compound **9** possesses the richest electrochemical behavior, exhibiting three reductive and two oxidative waves. The peaks at −1.20 and +1.50 V can be easily assigned to the Fe^{III} reduction and naphthalene oxidation, respectively. Assignments for the other three features are less certain. The process at −2.20 V is suggested to arise from the formation of the naphthalene radical anion. The remaining signals at +0.83 and −2.40 V appear to be unique to complex **9**. Since this is the only molecule in the series containing the TPA ligand, we tentatively assign these features to the oxidation and reduction, respectively, of the capping ligand. Unfortunately, we were unable to isolate a Zn analogue containing the TPA ligand to confirm these assignments.

A.2. Magnetism. Variable temperature magnetic susceptibility data were collected for compounds **8**−**11** in the solid state. All four complexes exhibited the antiferromagnetism expected for this class of molecules (Figure 4). The magnitude of the intramolecular coupling giving rise to this behavior can be quantified by fitting the data to a spin Hamiltonian of the form shown in eq 2,

$$\mathbf{H} = -2J\mathbf{S}_1\cdot\mathbf{S}_2 \qquad (2)$$

where $\mathbf{S}_1$ and $\mathbf{S}_2$ are the single-ion operators for Fe(1) and Fe(2), respectively, and J is the scalar exchange integral. The solid line in Figure 4 represents a fit of the data to an operator-equivalent form of eq 2. Data for all four complexes yielded coupling constants of -130 ± 10 cm^{-1}, values that lie well within the range typically found for the oxo-bridged diiron(III) structural motif.[18,19,30]

Magnetic susceptibilities were also determined using the Evans NMR method in order to assess the integrity of the dinuclear complexes in solution. The values obtained are significantly lower than the uncoupled value of 8.37 μ_B[31] and compare favorably with those measured for the solids

(29) The value reported in the literature was −0.76 V vs SCE. The value reported in the body of this paper has been converted to one vs Ag/$AgNO_3$ for ease of comparison by adding −0.273 V.

(30) Beer, R. H.; Tolman, W. B.; Bott, S. G.; Lippard, S. J. *Inorg. Chem.* **1991**, *30*, 2082−2092.

(31) The uncoupled value for the two high-spin iron(III) metal centers was calculated as $\mu_{eff} = [\Sigma_i (\mu_{eff})_i^2]^{1/2}$.

Table 3. Electrochemical Properties of Compounds **6** and **8**−**13**

compound	electrochemical potential (V)[a]
$C_{10}H_7-CH_2CO_2CH_3$ (**12**)	−1.60, +1.40[b]
$C_{10}H_6-(CH_2CH_2CO_2CH_3)_2$ (**6**)	+1.30[b], +1.50[b]
$[Zn_2(OH)(O_2CCH_2-C_{10}H_7)_2(TACN\text{-}Me_3)_2](ClO_4)$ (**13**)	−1.80[b], +1.50[b]
$[Fe_2O(O_2CCH_2-C_{10}H_7)(tren)_2](BPh_4)(NO_3)_2$ (**8**)	−0.60[b], −1.78[b], +1.46[b]
$[Fe_2O(O_2CCH_2-C_{10}H_7)(TPA)_2](ClO_4)_3$ (**9**)	−1.20[b], −2.20[b], −2.40[b], +0.83, +1.50[b]
$Fe_2O(O_2CCH_2-C_{10}H_7)_2(Tp)_2$ (**10**)	−1.07, −2.05, +1.30[b], +1.60[b]
$Fe_2O((O_2CCH_2CH_2)_2-C_{10}H_6)(Tp)_2$ (**11**)	−1.10[b], +1.40[b], +1.80[b]

[a] Measured in CH_3CN with 0.1 M $TBAPF_6$ as the supporting electrolyte. Potentials are reported vs $Ag/AgNO_3$. [b] Irreversible reduction or oxidation wave. The value refers to the potential at peak current.

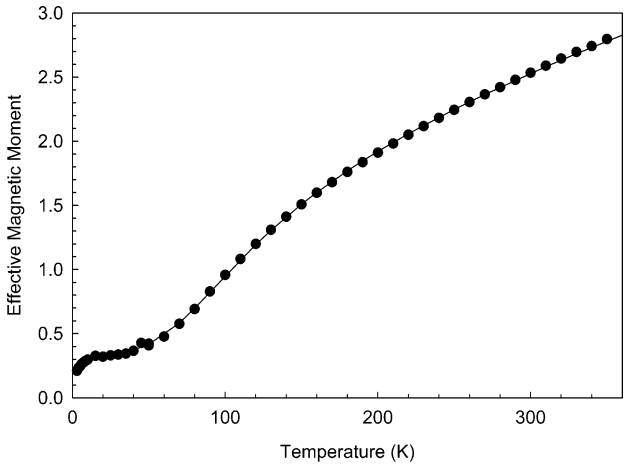

Figure 4. Plot of the effective magnetic moment vs temperature for $[Fe_2O(O_2CCH_2C_{10}H_7)(TPA)_2](ClO_4)_3$ (**9**) acquired in the solid state. The solid line represents a fit of the data to an operator-equivalent form of eq 2 with $J = -130$ cm^{-1}. See text for further details.

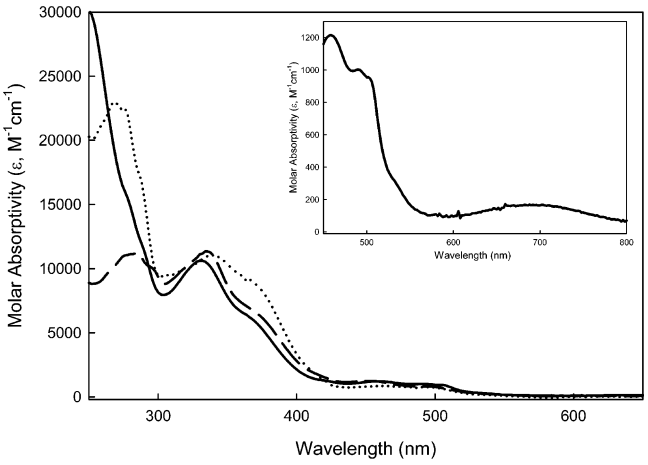

Figure 5. Electronic absorption spectra of $[Fe_2O(O_2CCH_2C_{10}H_7)(TPA)_2](ClO_4)_3$ (**9**, solid line), $Fe_2O(O_2CCH_2C_{10}H_7)_2(Tp)_2$ (**10**, dotted line), and $Fe_2O((O_2CCH_2CH_2)_2C_{10}H_6)(Tp)_2$ (**11**, dashed line) in CH_3CN solution at 298 K. The inset shows an expanded view of complex **9**, revealing the d−d band at ∼700 nm characteristic of oxo-bridged dinuclear Fe^{III} complexes.

at the same temperature. These data establish that the donor/acceptor assemblies all remain intact in solution.[32]

B. Steady-State and Time-Resolved Spectroscopies. The ground-state electronic absorption spectra of $[Fe_2O(O_2CCH_2-C_{10}H_7)(TPA)_2](ClO_4)_3$ (**9**), $Fe_2O(O_2CCH_2-C_{10}H_7)_2(Tp)_2$ (**10**), and $Fe_2O((O_2CCH_2CH_2)_2-C_{10}H_6)(Tp)_2$ (**11**) are illustrated in Figure 5. The visible and near-UV features of these complexes are all similar save for slight variations in the UV due to differing contributions from the aromatic capping ligands. Transitions associated with the oxo−diiron(III) cores are easily assigned based on the detailed analysis of the electronic structure of this class of compounds provided by Brown et al.[33] The weak band at ∼700 nm is assigned to a d−d transition. For high-spin d^5 metal ions all such transitions are spin-forbidden; however, in the present setting they gain intensity due to the electronic exchange coupling between the two Fe^{III} ions as well as intensity stealing from the higher-energy charge-transfer bands.[33−35] The iron−oxo core is also expected to give rise to bands in the 300−500 nm region corresponding to ligand-to-metal charge-transfer (LMCT) transitions associated with the bridging oxide.[33] These features are partly obscured in our complexes by the superposition of absorptions due to naphthalene as well as the capping ligands.

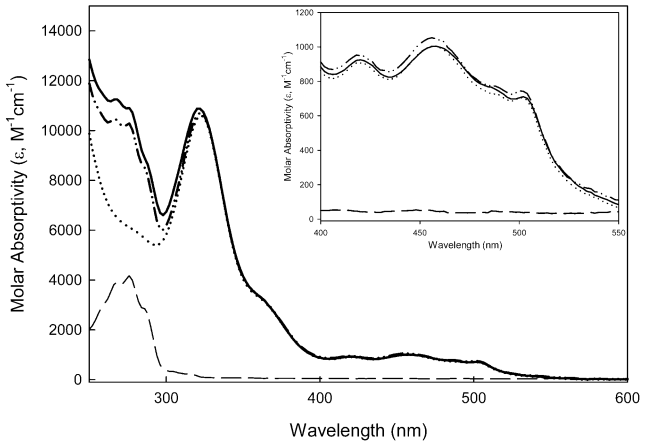

Figure 6. Electronic absorption spectra of $[Fe_2O(O_2CCH_2C_{10}H_7)(tren)_2]^{3+}$ (**8**, solid line), $[Fe_2O(O_2CCH_3)(tren)_2]^{3+}$ (dotted line), and 2-naphthylacetic acid (dashed line) in CH_3CN solution, along with a trace corresponding to the linear sum of the latter two spectra (dash-dot). The inset shows an expanded view of the LMCT features in the blue-to-midvisible region. See text for further details.

Figure 6 shows the absorption spectrum of compound **8**, along with the spectra of the free naphthalene acid and $[Fe_2O(O_2CCH_3)(tren)_2]^{3+}$. It can be seen that the visible and near-UV features of the naphthalene/iron−oxo assembly are reasonably approximated by a linear combination of the spectra of the latter two compounds.[36] Slight deviations are noted below 250 nm, largely due to changes in the breadth and intensity of the naphthalene-based transition near 220

(32) The integrity of the complexes in solution was also verified by chromatographic and electrospray mass spectroscopic techniques.
(33) Brown, C. A.; Remar, G. J.; Musselman, R. L.; Solomon, E. I. *Inorg. Chem.* **1995**, *34*, 688−717.

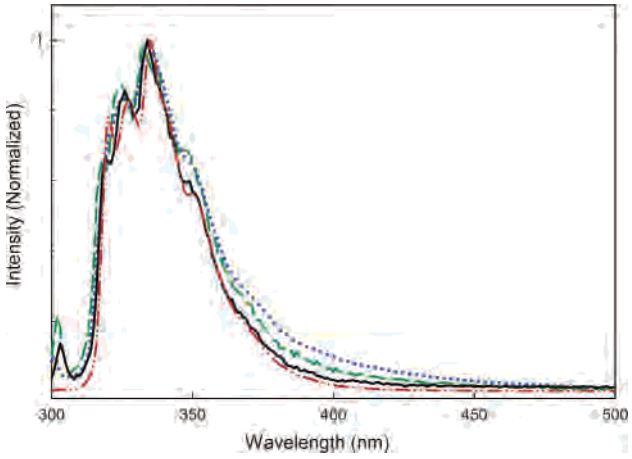

Figure 7. Corrected static emission spectra for $[Zn_2(OH)(O_2CCH_2C_{10}H_7)_2(TACN\text{-}Me_3)_2]^+$ (**13**, red dash-dot), $[Fe_2O(O_2CCH_2C_{10}H_7)(tren)_2]^{3+}$ (**8**, black solid), $[Fe_2O(O_2CCH_2C_{10}H_7)(TPA)_2]^{3+}$ (**9**, green dash), and $Fe_2O(O_2CCH_2C_{10}H_7)_2(Tp)_2$ (**10**, blue dot). Data were acquired in deoxygenated CH_3CN solution at 298 K following excitation at 280 nm. The sharp peak at ~310 nm in the spectra of compounds **8**−**11** is due to Raman scatter from the solvent.

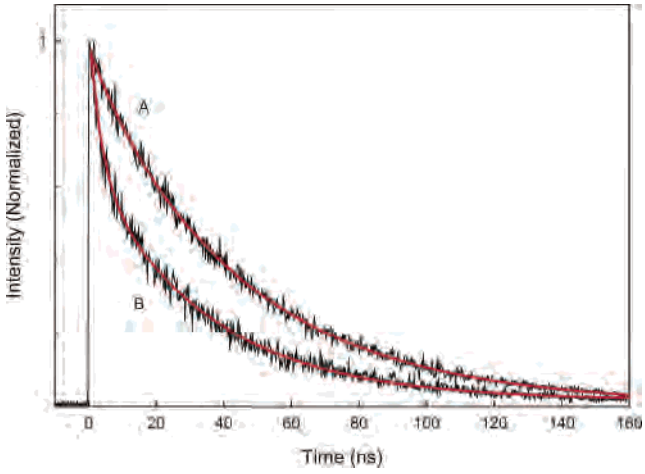

Figure 8. Normalized time-correlated single-photon counting emission data for $[Zn_2(OH)(O_2CCH_2C_{10}H_7)_2(TACN\text{-}Me_3)_2]^+$ (**13**, trace A) and $[Fe_2O(O_2CCH_2C_{10}H_7)(tren)_2]^{3+}$ (**8**, trace B) in deoxygenated CH_3CN solution. The solid lines correspond to fits of the data to exponential decay models. See the text for further details.

nm upon binding to the diiron(III) core. However, we do not consider this to be reflective of a significant change in the electronic structure of the naphthalene group in the assembled complex. The comparison presented in Figure 6 indicates that the relative contributions of the naphthalene group and the iron−oxo cluster to the absorption spectrum of the assembly are linearly independent, which in turn implies relatively weak electronic coupling between these components in the molecule's ground state.

B.1. Steady-State and Time-Resolved Emission. Emission spectra for all four Fe-containing complexes as well as that of $[Zn_2(OH)(O_2CCH_2{-}C_{10}H_7)_2(TACN\text{-}Me_3)_2](ClO_4)$ were obtained at 298 K in CH_3CN. The spectral profiles of all five complexes are quite similar; representative examples are illustrated in Figure 7. On the basis of spectral profile and observed lifetimes (vide infra), the emission is assigned to the $S_1 \rightarrow S_0$ fluorescence of naphthalene.[37,38] Qualitatively, the emission intensities of all four iron-containing assemblies are significantly attenuated relative to both methyl-2-naphthyl acetate ($\phi_r = 0.16$) and $[Zn_2(OH)(O_2CCH_2{-}C_{10}H_7)_2(TACN\text{-}Me_3)_2]^+$ ($\phi_r = 0.12$). Quantifying this difference is somewhat difficult due to absorptive interferences from both the iron−oxo core and, in the cases of complexes **8**−**11**, the aromatic capping ligands. However, given the preceding discussion, the absorbance of the naphthalene group at the excitation wavelength ($\lambda_{ex} = 280$ nm) can be estimated from the ratio of the molar absorptivities of the naphthalene (obtained from either methyl-2-naphthyl acetate or complex **13**) to that of the complete iron−oxo−naphthalene assembly. When the measured absorbance of complex **8** is multiplied by this ratio (i.e., $\epsilon_{\lambda=280}{}^{naph}/\epsilon_{\lambda=280}{}^{8} = 0.343$), a radiative quantum yield of 0.011 is calculated. Emission from the S_1 state of naphthalene in complex **8** therefore appears to be quenched by roughly an order of magnitude relative to that of both the free ligand and $[Zn_2(OH)(O_2CCH_2{-}C_{10}H_7)_2(TACN\text{-}Me_3)_2]^+$. Similar results are found for complexes **9**−**11**.

Additional details concerning quenching of the S_1 state were obtained through time-correlated single-photon counting emission measurements on all four iron complexes as well as $[Zn_2(OH)(O_2CCH_2{-}C_{10}H_7)_2(TACN\text{-}Me_3)_2]^+$. The Zn complex represents an ideal model for the photophysics of this system since it is essentially isostructural to the Fe-containing molecules of interest but cannot engage in electron or energy transfer with the naphthalene group. Emission decay from $[Zn_2(OH)(O_2CCH_2{-}C_{10}H_7)_2(TACN\text{-}Me_3)_2]^+$ could be fit to a single-exponential model with $\tau_{obs} = 45 \pm 2$ ns, corresponding to radiative and nonradiative decay rate constants of $k_r = 2.65 \pm 0.2 \times 10^6$ s^{-1} and $k_{nr} = 1.95 \pm 0.2 \times 10^7$ s^{-1}, respectively. These values are consistent with the assignment of $S_1 \rightarrow S_0$ for the emission of this compound. On the basis of this observation, all four of the iron complexes reveal evidence of quenching with S_1 lifetimes of $\tau_{obs}{}^{S_1} = 36 \pm 2$, 32 ± 4, 30 ± 5, and 39 ± 3 ns for $[Fe_2O(O_2CCH_2{-}C_{10}H_7)(tren)_2]^{3+}$ (**8**), $[Fe_2O(O_2CCH_2{-}C_{10}H_7)(TPA)_2]^{3+}$ (**9**), $Fe_2O(O_2CCH_2{-}C_{10}H_7)_2(Tp)_2$ (**10**), and $Fe_2O((O_2CCH_2CH_2)_2{-}C_{10}H_6)(Tp)_2$ (**11**), respectively. The degree of quenching observed based on these lifetimes is admittedly small but is well outside experimental error as the comparison in Figure 8 demonstrates.

There is clearly a significant disparity between the degree of quenching inferred from the time-resolved data and the emission quantum yields discussed previously. Taking the data on complex **8** as an example, the reduction in lifetime suggests a ~20% quenching of the S_1 state relative to that of $[Zn_2(OH)(O_2CCH_2{-}C_{10}H_7)_2(TACN\text{-}Me_3)_2]^+$, whereas the emission quantum yield data suggest a value closer to a factor of ~10. The simplest explanation for this apparent lack of internal consistency is an internal filtering effect associated with the low-energy absorptions of the iron−oxo core. An

(34) McCarthy, P. J.; Gudel, H. U. *Coord. Chem. Rev.* **1988,** *88,* 69.
(35) Solomon, E. I. Department of Chemistry, Stanford University. Personal Communication, October 17, 2003.
(36) Qualitatively similar results were also obtained for complexes **9**−**11**.
(37) Berlmane, I. B. *Handbook of Fluorescence Spectra of Aromatic Molecules,* 2nd ed.; Academic Press: New York, 1971.
(38) Birks, J. B. *Photophysics of Aromatic Molecules*; Wiley-Interscience: New York, 1970.

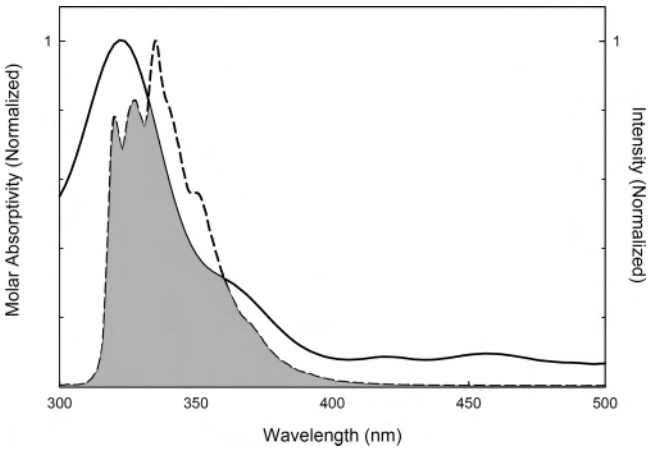

Figure 9. Overlay of the emission spectrum of $[Zn_2(OH)(O_2CCH_2C_{10}H_7)_2(TACN\text{-}Me_3)_2]^+$ (**13**, dashed line) with the absorption spectrum of $[Fe_2O(O_2CCH_2C_{10}H_7)(tren)_2]^{3+}$ (**8**, solid line). The shaded region represents the area of overlap between the two spectra that allows for dipolar energy transfer from the naphthyl group to the iron−oxo core.

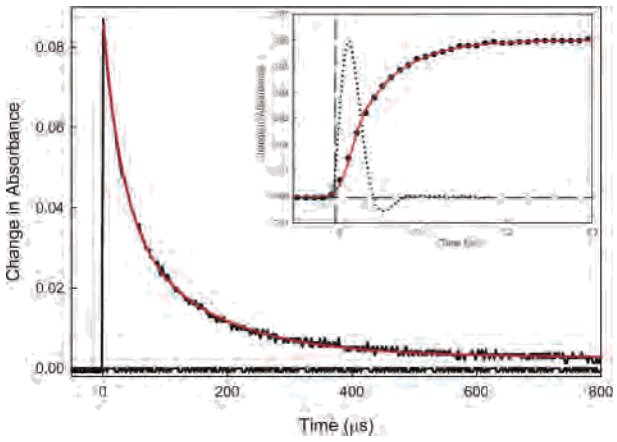

Figure 10. Nanosecond time-resolved absorption data for $[Zn_2(OH)(O_2CCH_2C_{10}H_7)_2(TACN\text{-}Me_3)_2]^+$ (**13**) in deoxygenated CH_3CN solution at 420 nm following excitation at 266 nm. The solid line corresponds to a fit of the data, indicating a lifetime of $\tau = 90 \pm 10$ μs for the lowest-energy triplet state (T_1) of naphthalene. The offset from baseline following the decay reflects slight decomposition of the sample that occurs due to photolysis. The inset shows an expanded view at early times, along with a plot of the instrument response function of the spectrometer (dotted curve). The fit indicates a rise time for the T_1 absorption of $\tau = 50 \pm 10$ ns.

overlay of the emission spectrum of $[Zn_2(OH)(O_2CCH_2-C_{10}H_7)_2(TACN\text{-}Me_3)_2]^+$ with the absorption spectrum of $[Fe_2O(O_2CCH_3)(tren)_2]^{3+}$ is shown in Figure 9. It can be seen that reabsorption of emission by the iron−oxo complex is potentially significant even under the optically dilute conditions under which the emission data were acquired. Qualitatively it seems quite reasonable to us that this reabsorption could account for the factor of 5 loss in the observed emission intensity; this phenomenon would have no impact on the lifetime measured for S_1. The alternative explanation, namely, a loss in S_1 yield due to ultrafast reactivity from the S_2 state of naphthalene, is not unequivocally ruled out but is deemed unlikely given the rates observed for reaction from S_1.

B.2. Time-Resolved Absorption. Transient absorption experiments were undertaken in an effort to further characterize the excited-state properties of these compounds. The excited-state singlet (S_1), triplet (T_1), and radical cation absorption spectra of naphthalene are well-known and characterized;[39−41] these provide us with the optical markers necessary to distinguish among the various quenching processes that could be operative in these assemblies.

Upon excitation at 266 nm, $[Zn_2(OH)(O_2CCH_2-C_{10}H_7)_2(TACN\text{-}Me_3)_2]^+$ reveals a number of significant features. Information at short probe wavelengths ($\lambda_{probe} < 400$ nm) is largely obscured due to emission from the S_1 state; however, correcting for the emission reveals a weak transient feature with a lifetime of ~50 ns. This is consistent with the emission lifetime of 45 ± 2 ns obtained from TCSPC measurements and is therefore assigned to the decay of the S_1 state. At 420 nm an additional signal is observed, the data for which are shown in Figure 10. The lifetime of $\tau_{obs} = 90 \pm 10$ μs coupled with its spectral profile supports assigning this feature to the lowest-energy triplet excited state of naphthalene.

A closer inspection of the data at $\lambda_{probe} = 420$ nm reveals a rise time for $T_1 \rightarrow T_n$ absorption feature of 50 ± 10 ns (Figure 10, inset), suggesting an intersystem crossing rate constant of $k_{isc} \sim 2 \times 10^7$ s^{-1}. The static and time-resolved emission data on $[Zn_2(OH)(O_2CCH_2-C_{10}H_7)_2(TACN\text{-}Me_3)_2]^+$ indicated a nonradiative decay rate constant of $k_{nr} = 1.95 \pm 0.2 \times 10^7$ s^{-1} for the S_1 state of this compound. The $S_1 \rightarrow T_1$ conversion therefore comprises essentially all of the nonradiative decay dynamics associated with the S_1 state of the Zn model system.

Nanosecond time-resolved absorption data for all four iron−oxo complexes were acquired in CH_3CN solution at 298 K. At the outset, it should be noted that these experiments suffered from the same problem of overlapping absorption features that rendered the radiative quantum yields difficult to obtain. The absorption for each of these assemblies at 266 nm (the only UV wavelength experimentally available) is dominated by the iron−oxo species. Although previous measurements on the iron−oxo core in the absence of the naphthalene chromophore showed that there were no transient features on the nanosecond time scale,[13] the relative absorption cross sections nevertheless reduces the fraction of naphthalene molecules that are excited. This directly translates into a reduction in the signal-to-noise of the transient absorption data.

Poor signal-to-noise notwithstanding, the transient absorption features for all four iron−oxo−naphthalene assemblies were reminiscent of those of the Zn model complex with regard to the S_1 state. For example, all of the compounds revealed weak absorptions centered at ~380 nm. Although the exceedingly small amplitude of the signal precluded quantifying the kinetics, lifetimes were qualitatively consistent with the $S_1 \rightarrow S_0$ decay observed in the time-resolved emission experiments for all molecules studied. Spectral profiles associated with the triplet state in the iron−oxo systems matched that of the Zn complex. In the case of

(39) Niederalt, C.; Grimme, S.; Peyerimhoff, S. D. *Chem. Phys. Lett.* **1995**, *245*, 455−462.
(40) Birks, J. B. *Organic Molecular Photophysics*; John Wiley & Sons: New York, 1975; Vol. 2.
(41) Sakamoto, M.; Cai, X.; Hara, M.; Fujitsuka, M.; Majima, T. *J. Am. Chem. Soc.* **2004**, *126*, 9709−9714.

Table 4. Singlet (τ_S) Lifetimes, Radiative ($k_r^{S_1}$) and Nonradiative ($k_{nr}^{S_1}$) Decay Constants, and Triplet (τ_T) Lifetimes for the Complexes Described in This Study

compound	τ_S (ns)[a]	k_r (s^{-1})[b]	k_{nr} (s^{-1})[b]	τ_T (μs)[c]
$C_{10}H_7-CH_2CO_2CH_3$ (**12**)	58 ± 1	2.2×10^6	1.5×10^7	48 ± 1
$C_{10}H_6-(CH_2CH_2CO_2CH_3)_2$ (**6**)	50 ± 3	3.2×10^6	1.7×10^7	30 ± 3
$[Zn_2(OH)(O_2CCH_2-C_{10}H_7)_2(TACN\text{-}Me_3)_2](ClO_4)$ (**13**)	45 ± 2	2.65×10^6	1.95×10^7	90 ± 10[d]
$[Fe_2O(O_2CCH_2-C_{10}H_7)(tren)_2](BPh_4)(NO_3)_2$ (**8**)	36 ± 2		2.5×10^7[e]	5 ± 2
$[Fe_2O(O_2CCH_2-C_{10}H_7)(TPA)_2](ClO_4)_3$ (**9**)	32 ± 4		2.8×10^7[e]	3 ± 1
$Fe_2O(O_2CCH_2-C_{10}H_7)_2(Tp)_2$ (**10**)	30 ± 5		3.1×10^7[e]	5 ± 1
$Fe_2O((O_2CCH_2CH_2)_2-C_{10}H_6)(Tp)_2$ (**11**)	39 ± 3		2.3×10^7[e]	3 ± 1

[a] Singlet lifetimes were measured by TCSPC in deoxygenated CH_3CN solution. A small fluorescent impurity arising from the solvent was detected in the data for complexes **8**−**11** and was incorporated as a fixed parameter in the fits. See the text for further details. [b] Values for k_r and k_{nr} were calculated as described in the text for complexes **8**−**11**. Propagated error bars are estimated at 10−15%. [c] Triplet lifetimes were measured by nanosecond transient absorption spectroscopy in deoxygenated CH_3CN solution. [d] Compound **13** showed biphasic kinetics associated with the decay of the triplet state. The shorter component (28 ± 9 μs) represented a minor fraction of the overall signal. Its origin is still under investigation. [e] Values for k_{nr} were calculated by fixing k_r to the value obtained for complex **13**. See the text for further details.{

Table 5. Energy Transfer Rates for Complexes **8**−**11**

compound	$S_1 \rightarrow Fe_2O$ core (s^{-1})[a]	$T_1 \rightarrow Fe_2O$ core (s^{-1})[b]
$[Fe_2O(O_2CCH_2-C_7H_{10})(tren)_2](BPh_4)(NO_3)_2$ (**8**)	$5.6 \pm 5 \times 10^6$	$2 \pm 1 \times 10^5$
$[Fe_2O(O_2CCH_2-C_{10}H_7)(TPA)_2](ClO_4)_3$ (**9**)	$9.0 \pm 5 \times 10^6$	$3.5 \pm 1 \times 10^5$
$Fe_2O(O_2CCH_2-C_{10}H_7)_2(Tp)_2$ (**10**)	$11 \pm 6 \times 10^6$	$2.0 \pm 0.5 \times 10^5$
$Fe_2O((O_2CCH_2CH_2)_2-C_{10}H_6)(Tp)_2$ (**11**)	$3.5 \pm 3 \times 10^6$	$3.5 \pm 1 \times 10^5$

[a] Calculated from eq 4b. For each entry, the error bars cited fully encompass those listed in Table 4 for the measured S_1 lifetimes of both the iron−oxo complex and the Zn model compound (complex **13**). [b] Calculated from eq 5. For each entry, the error bars cited fully encompass those listed in Table 4 for the measured T_1 lifetimes of both the iron−oxo complex and the Zn model compound (complex **13**).

complex **8** (which suffers the least from competing absorptions, vide supra), we were also able to detect the formation of the $T_1 \rightarrow T_n$ absorption at $\lambda_{probe} = 420$ nm. The rise time for this feature was similar to that of the Zn complex **13**, indicating a similar rate for the $S_1 \rightarrow T_1$ intersystem crossing in the iron−naphthalene systems.[42]

The most significant observation in the transient absorption spectroscopy of the iron-containing assemblies was the order-of-magnitude reduction in their T_1 state lifetimes relative to that of $[Zn_2(OH)(O_2CCH_2-C_{10}H_7)_2(TACN\text{-}Me_3)_2]^+$: time constants for the decay of the long-lived excited state were in the range of $\tau_{obs}^{T_1} = 5 \pm 2$ μs for all four complexes studied (Table 4). These data indicate that the iron−oxo core quenches the T_1 state of naphthalene with an efficiency in excess of 90%.

C. Mechanistic Considerations: Energy versus Electron Transfer. The data we have acquired allow us to construct an overall picture of the photophysics of this class of molecules. On the left side of Figure 11 is an energy level diagram for the relevant electronic states of naphthalene. Initial population of the S_2 state leads to rapid formation of S_1, which subsequently decays via radiative coupling to the ground state (k_r) or intersystem crossing to T_1 (k_{isc}). The oxo-bridged diiron(III) core introduces two new reaction pathways leading to quenching of the S_1 and T_1 states of naphthalene ($k_q^{S_1}$ and $k_q^{T_1}$, respectively). The observed rate of decay of the S_1 state of naphthalene for the iron−oxo assemblies is given by

$$k_{obs}^{S_1}(Fe) = k_r^{S_1} + k_{nr}^{S_1} + k_{isc} + k_q^{S_1} \quad (3)$$

where all of the rates are as previously defined. Applying the reasonable assumption that k_r for naphthalene does not differ significantly when bound to a Zn_2^{II} versus an Fe_2^{III} core, combined with the fact that k_{isc} was determined to be the same for both the Zn- and Fe-containing assemblies,[42] the quenching rate constant can be expressed as the difference between the observed rate constants for decay for the Zn and Fe complexes (eq 4).

$$k_q^{S_1} = k_{obs}^{S_1}(Fe) - k_r^{S_1} - k_{nr}^{S_1} - k_{isc} \quad (4a)$$

$$= k_{obs}^{S_1}(Fe) - k_{obs}^{S_1}(Zn) \quad (4b)$$

Similar arguments hold for the quenching of the T_1 state, eq 5.

$$k_q^{T_1} = k_{obs}^{T_1}(Fe) - k_{obs}^{T_1}(Zn) \quad (5)$$

The calculated singlet and triplet quenching rates for complexes **8**−**11** are given in Table 5. The rates for quenching of the S_1 state exceed that of the T_1 state by more than an order of magnitude, although both are relatively small given the intimate nature of these covalently linked assemblies.

Both energy and electron transfer from naphthalene to the iron−oxo core are thermodynamically viable mechanisms in these complexes. Electron transfer from naphthalene will yield a naphthalene radical cation and a reduced $Fe^{II}Fe^{III}$ cluster as photoproducts. However, the transient absorption experiments just described failed to reveal any feature that could be attributed to either of these two photoproducts. In particular, no transient absorption was detected for any of

(42) Kilsa et al. have reported an enhancement in the rate of intersystem crossing following the introduction of high-spin Fe^{III} into a porphyrin-based donor/acceptor system: Kilsa, K.; Kajanus, J.; Larsson, S.; Macpherson, A. N.; Martensson, J.; Albinsson, B. *Chem. Eur. J.* **2001**, *7*, 2122−2133. Our data indicate that k_{isc} is the same, within experimental error, for both the Zn_2 and Fe_2 complexes. Although our signal-to-noise is such that we cannot exclude a slight perturbation to the k_{isc}, any increase would have to be significantly less than the factor of 2 that these authors observe in their system.

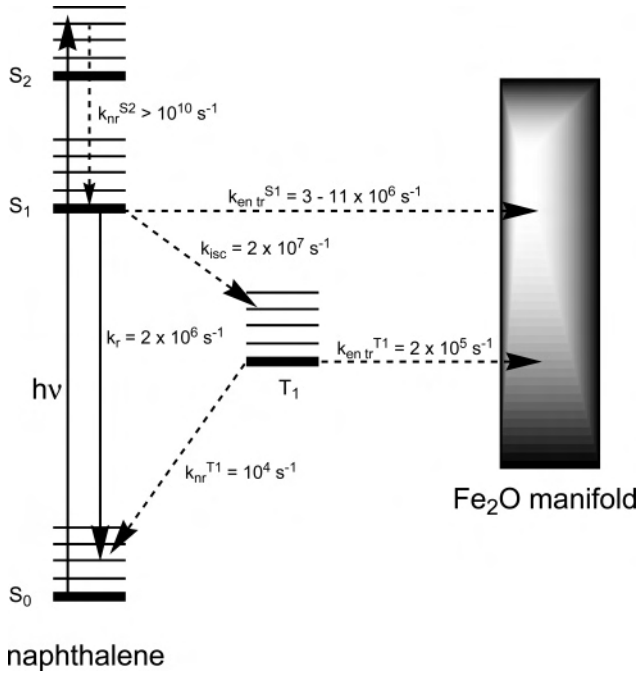

Figure 11. Energy level diagram summarizing the results of the kinetic studies on naphthalene-containing iron−oxo cluster assemblies.

the complexes near 600 nm where the naphthalene radical cation is expected to absorb.[40] It should be acknowledged that the absorption cross sections for both naphthalene$^{+\bullet}$ and the mixed-valence $Fe^{II}Fe^{III}$ species are expected to be small.[39,41,43,44] We therefore cannot state unequivocally that there is no electron transfer occurring in these systems upon photoexcitation. Nevertheless, there is no experimental evidence to support such a mechanism.

In our estimation, a far more likely explanation for dynamic quenching of both the S_1 and T_1 states of naphthalene is energy transfer to the dinuclear Fe^{III} core. The two common mechanisms are dipolar (Förster) and through-bond superexchange (Dexter).[38] The literature is replete with examples of Förster transfer in organic as well as inorganic systems. For example, phenanthrene/naphthalene bichromophoric systems have been shown to undergo dipolar energy transfer from their singlet and triplet states.[43,45,46] Several intramolecular inorganic/organic hybrid systems have also been described which exhibit analogous reactivity.[47−49] In particular, Dexter transfer has been unambiguously identified in a (diimine)$Re^{I}(CO)_3$−[CpM^{II}(arene)] system (M = Fe or Ru).[50] In this case, the authors were able to determine the energy transfer mechanism using variable temperature studies that allowed them to rule out dipole−dipole or dipole−multipole coupling. This latter study represents the exception and not the rule, as experimentally distinguishing between dipolar and exchange pathways is usually quite difficult. The optical properties and availability of low-lying electronic states associated with the iron−oxo core in the assemblies we are considering here make both mechanisms possible and thus hard to differentiate.

The probability of Förster energy transfer can be estimated from the overlap of the emission spectrum of the donor (i.e., naphthalene) with the absorption spectrum of the acceptor (the iron−oxo cluster). Figure 9 shows quite clearly that the overlap requirement in these systems is satisfied suggesting that Förster transfer from the S_1 state of naphthalene should be highly favored.[51,52] However, the remarkably slow rate of energy transfer observed for these systems (Table 5) tends to belie this expectation. We can think of two possible explanations for this observation. The first is an orientation effect. In addition to the overlap factor described above, the rate of energy transfer is sensitive to the relative orientation of the donor and acceptor transition dipoles: this orientation factor is given by κ. For a donor/acceptor system undergoing free rotation (i.e., the isotropic limit), a value of $\kappa = {}^2/_3$ is expected. In general, however, κ will depend strongly on the angle between the two dipoles and can take on any value from 0 to 4.[40,51,52] Based on our X-ray structures and spectral overlap considerations, we estimate using the Förster equation that an orientation factor of $\kappa \sim 0.03$ would be required in order to account for our experimental data.[53] We do not have the single-crystal absorption and emission data necessary to specify the orientations of the transition dipoles in these molecules, but we can make reasonable estimates based on the nature of the transitions involved. The spectral features of the iron−oxo core that overlap with the naphthalene emission correspond to oxo-to-iron LMCT transitions. It is therefore likely that the relevant absorptive dipole of the acceptor will lie in the $Fe-O_{bridge}-Fe$ plane. The precise disposition of the emission dipole of the naphthyl group is unclear; however, it will certainly lie in the plane of that molecule. An examination of the X-ray structures for compounds **8**, **9**, and **10** reveals angles between the naphthalene and Fe−O−Fe planes of 82°, 96°, and 89°, respectively. To the extent that the relative positions of the components are retained in solution,[53] these angles are consistent with the near-orthogonality implied by the small value of κ.

A second possibility concerns the applicability of the Förster model for quantifying energy transfer rates in this system. This question arises due to the close proximity of

(43) Shida, T. *Electronic Absorption Spectra of Radical Ions*; Elsevier: New York, 1988.
(44) Reductive spectroelectrochemical measurements carried out on several of the iron−oxo assemblies revealed weak absorptions in the mid-visible, but the instability of the $Fe^{II}Fe^{III}$ species prevented further characterization.
(45) McGimpsey, W. G.; Samaniego, W. N.; Chen, L.; Wang, F. *J. Phys. Chem. A* **1998**, *102*, 8679−8689.
(46) Tan, Z.; Kote, R.; Samaniego, W. N.; Weininger, S. J.; McGimpsey, W. G. *J. Phys. Chem. A* **1999**, *103*, 7612−7620.
(47) Indelli, M. T.; Ghirotti, M.; Prodi, A.; Chiorboli, C.; Scandola, F.; McClenaghan, N. D.; Puntoriero, F.; Campagna, S. *Inorg. Chem.* **2003**, *42*, 5489−5497.
(48) Simon, J. A.; Curry, S. L.; Schmehl, R. H.; Schatz, T. R.; Piotrowiak, P.; Jin, X.; Thummel, R. P. *J. Am. Chem. Soc.* **1997**, *119*, 11012−11022.
(49) Wilson, G. J.; Launikonis, A.; Sasse, W. H. F.; Mau, A. W.-H. *J. Phys. Chem. A* **1997**, *101*, 4860−4866.
(50) Wang, Y.; Schanze, K. S. *Inorg. Chem.* **1994**, *33*, 1354−1362.
(51) Yardley, J. T. *Introduction to Molecular Energy Transfer*; Academic Press: New York, 1980.
(52) Van Der Meer, B. W.; Coker, G., III; Chen, S.-Y. S. *Resonant Energy Transfer, Theory and Data*; VCH Publishers: New York, 1994.
(53) It is unlikely that the naphthyl group will be static in solution (e.g., the group can rotate about the methylene carbon at the 2-position); however, the structural constraints of these assemblies will significantly hinder the isotropic motion necessary to recover a value of $\kappa = {}^2/_3$.

the donor (naphthalene) to the acceptor (iron−oxo core) and has been considered in detail by Rossky for polymer/porphyrin assiblies[54] as well as Fleming in the context of photosynthesis.[55] At issue is the break-down of the point−dipole approximation endemic to the Förster model. At sufficiently short energy transfer distances, i.e., when the magnitudes of the transition dipoles are comparable to the donor−acceptor separation, the Förster equation can dramatically overestimate the rate of energy transfer, in at least one case by more than two orders of magnitude.[54] Put another way, the favorable overlap evident in Figure 9 may not translate into an efficient energy transfer rate—at least one predicted by the Förster equation—because the donor and acceptor are too close. Viewed in the context, the anomalously small value of κ inferred in the preceding discussion could in part be a numerical artifact reflecting this situation. We suggest that a combination of both of these factors are responsible for the surprisingly slow rate of energy transfer from S_1 in these systems.

Energy transfer from the T_1 state presents a somewhat different mechanistic picture. For a dipolar mechanism to be operative, the transition dipoles of both the donor and the acceptor must have appreciable magnitude. Our detection threshold for emission allows us to easily measure spectra of systems possessing radiative quantum yields of less than 1%. The lack of any observable phosphorescence from complex **13** coupled with the measured lifetime of the T_1 state therefore allows us to place an upper limit of $\sim 10^2\ s^{-1}$ on the value of $k_r^{T_1}$. This implies an exceedingly small magnitude for the $T_1 \rightarrow S_0$ transition dipole and a correspondingly small value for the spectral overlap integral relative to what is observed for the S_1 state. The reduction in k_r by $\sim 10^4$ is at odds with the quenching data that indicate only a 10-fold decrease in $k_{en\ tr}$ for the T_1 state. Given these observations, a different mechanism for energy transfer from the T_1 state compared to that of the S_1 state seems likely. We therefore suggest that Dexter transfer to the iron−oxo core is the origin for the reduction in lifetime observed for the naphthalene T_1 state in complexes **8**−**11**.

Concluding Comments: On the Origin of Dual Reactivity

The syntheses, structures, and physical properties of intramolecular donor/acceptor systems containing naphthalene donors and antiferromagnetically coupled diiron(III) cores as acceptors have been described. It was found that photoexcitation of the naphthalene chromophore resulted in intramolecular electronic energy transfer to the Fe^{III}_2 core from both the lowest-lying singlet (S_1) and triplet (T_1) excited states of naphthalene. A dipolar mechanism for quenching of the S_1 state appears most likely, whereas the lack of appreciable phosphorescence coupled with the measured rates of energy transfer points to Dexter exchange as the origin of the >90% quenching of the T_1 state.

Aromatic organic chromophores such as naphthalene are known to undergo intramolecular energy transfer from their singlet or triplet states when an appropriate acceptor is present.[40] The observation of both singlet *and* triplet energy transfer involving the same donor/acceptor pair is rather unusual. We believe this has two possible origins: (1) the slow rate of energy transfer from S_1 and/or (2) the electronic structure of the exchange-coupled acceptor. The first is simply an acknowledgment of the fact that the quenching rate for the S_1 state in these systems is quite low. As discussed above, this appears to be due to poor alignment of the transition dipoles for the naphthyl and iron−oxo groups and/or break-down in the point−dipole appoximation for Förster transfer. Regardless of its origin, a consequence of this unusually slow rate is that intersystem crossing to the T_1 state—which we directly observed—is a kinetically competitive pathway for deactivation of the S_1 state in the iron−oxo assemblies. It could be argued that in most systems triplet quenching is not observed simply because intersystem crossing is not competitive with the S_1 quenching pathway, and thus the triplet state is never formed. As it stands, in our systems the triplet is formed in ~85% yield and is therefore available to engage in energy transfer.

The kinetics represent only part of the story, however: the other issue that must be considered is the electronic structure of the acceptor, i.e., the exchange-coupled iron−oxo core. In general, energy transfer, whether by a dipolar or exchange mechanism, must conserve angular momentum. In the simplest terms, this means that the angular momentum space spanned by the reactants must intersect the angular momentum space spanned by the products. In the limit that the total spin S is a good quantum number, an energy transfer process is formally allowed if there exist spin states in both the reactant and product space for which $\Delta S = 0$ and $\Delta G_0^{R\rightarrow P} < 0$. The $S_1 \rightarrow S_0$ relaxation in naphthalene therefore requires coupling to an excited state of the acceptor that lies below the S_1 state of naphthalene and has the same spin multiplicity as the acceptor's ground state. In the context of the Förster model, this means coupling to a spin-allowed transition of the acceptor, e.g., Figure 9. Momentum conservation for energy transfer from the T_1 of naphthalene is more facile due to the change in spin multiplicity associated with the $T_1 \rightarrow S_0$ transition. The criterion can be satisfied for any excited state of the acceptor with spin S_{A^*} such that $|S_{A^*}| = |S_A| \pm 1$. For example, if the acceptor had a ground state of $S = {}^5/_2$, any excited states having $S^* = {}^3/_2$, ${}^5/_2$, or ${}^7/_2$ whose zero-point energies lies below the T_1 state could act as acceptors, at least in principle.[56]

(54) Wong, K. F.; Bagchi, B.; Rossky, P. J. *J. Phys. Chem. A* **2004**, *108*, 5725−5763.

(55) (a) Fleming, G. R.; Scholes, G. D. *Nature* **2004**, *431*, 256−257. (b) Jordanides, X. J.; Scholes, G. D.; Fleming, G. R. *J. Phys. Chem. B* **2001**, *105*, 1652.

(56) In this example only the $S^* = {}^5/_2$ state may have sufficient oscillator strength to allow for appreciable dipolar coupling. States having $S^* = {}^3/_2$ and $S^* = {}^7/_2$ would give rise to weak, spin-forbidden absorptions and would therefore be more likely to engage in Dexter rather than Förster transfer.

Given the preceding discussion, it seems clear that the more complex the structure of the acceptor in terms of the density and diversity of electronic states, the more likely it is that momentum conservation for energy transfer involving donor excited states of differing spin multiplicity can be simultaneously satisfied for a single donor/acceptor pair. We believe this may be responsible, at least in part, for the dual reactivity observed in the systems we have described in this report. The electron exchange interaction with the iron−oxo core significantly expands the palette of spin states available as energy traps, particularly within the ground-state manifold: this will translate into a large number of spin-allowed pathways with significant driving forces for energy transfer. The data we have presented do not allow us to make any definitive statements along these lines, but they nevertheless suggest that the modulation of electronic structure afforded by Heisenberg spin coupling could provide a useful tool for exploring the role of spin polarization in energy as well as electron-transfer reactions.[57] Work along these lines is presently underway.

Acknowledgment. The authors thank Professor Gary Blanchard for use of the time-correlated single-photon counting spectrometer and for a number of fruitful discussions. This work was supported with funds from Michigan State University.

Supporting Information Available: Crystallographic data in cif format. This material is available free of charge via the Internet at http://pubs.acs.org.

IC0506761

(57) For a recent study of electron-transfer involving spin-coupled metals, see: Obata, M.; Tanihara, N.; Nakai, M.; Haradag, M.; Akimoto, S.; Yamazaki, I.; Ichimura, A.; Kinoshita, I.; Mikuriya, M.; Hoshino, M.; Yano, S. *Dalton Trans.* **2004**, 3283−3287.